Ribosomal RNA 2′-*O*-methylations regulate translation by impacting ribosome dynamics

Sohail Khoshnevis[a,1] 📷, R. Elizabeth Dreggors-Walker[a,b], Virginie Marchand[c], Yuri Motorin[d] 📷, and Homa Ghalei[a,1] 📷

Protein synthesis by ribosomes is critically important for gene expression in all cells. Ribosomal RNAs (rRNAs) are marked by numerous chemical modifications. An abundant group of rRNA modifications, present in all domains of life, is 2′-*O*-methylation guided by box C/D small nucleolar RNAs, which are part of small ribonucleoprotein complexes (snoRNPs). Although 2′-*O*-methylations are required for the proper production of ribosomes, the mechanisms by which these modifications contribute to translation have remained elusive. Here, we show that a change in box C/D snoRNP biogenesis in actively growing yeast cells results in the production of hypo-2′-*O*-methylated ribosomes with distinct translational properties. Using RiboMethSeq for the quantitative analysis of 2′-*O*-methylations, we identify site-specific perturbations of the rRNA 2′-*O*-methylation pattern and uncover sites that are not required for ribosome production under normal conditions. Characterization of the hypo-2′-*O*-methylated ribosomes reveals significant translational fidelity defects, including frameshifting and near-cognate start codon selection. Using rRNA structural probing, we show that hypo-2′-*O*-methylation affects the inherent dynamics of the ribosomal subunits and impacts the binding of eukaryotic translation initiation factor 1, thereby causing translational defects. Our data reveal an unforeseen spectrum of 2′-*O*-methylation heterogeneity in yeast rRNA and suggest a significant role for rRNA 2′-*O*-methylation in regulating cellular translation by controlling ribosome dynamics and ligand binding.

2′-*O*-methylation | rRNA modification | ribosome biogenesis | ribosome dynamics | translation regulation

RNA molecules are subject to co- and posttranscriptional modifications, which expand their chemical and topological properties (1, 2). Methylation of the 2′-*O* position of the ribose moiety of nucleotides is a highly abundant RNA modification found in all four types of ribonucleotides in both coding and noncoding RNAs in all domains of life (3). Ribosomal RNAs (rRNAs) are a major target of ribose 2′-*O* methylations, with 55 2′-*O*-methylation sites identified in budding yeast and ~110 in humans. Although rRNA 2′-*O*-methylations are critical for the proper production of ribosomes and accurate protein translation, their precise molecular contributions and mechanism of function are unknown (3–8). The chemical properties of 2′-*O*-methylations and the observations made based on their contributions to the structure of the ribosome have suggested a role for rRNA modifications in local and global stabilization of the rRNA structure (1, 6, 7, 9, 10). Moreover, rRNA modifications contribute to the interactions of ligands with the ribosome (11–13). Studies of modified nucleotides and RNA oligonucleotides have pointed to the importance of 2′-*O*-methylation in the stabilization of RNA structure by favoring the 3′-endo configuration of the ribose moiety and restricting the rotational freedom of the 3′-phosphate (14–19). However, how methylations of the rRNA backbone contribute to ribosome biogenesis and function remains largely unknown to date (4, 5, 20).

In eukaryotes and archaea, box C/D small nucleolar RNAs (snoRNAs) guide the 2′-*O*-methylation of rRNA sites by base pairing to specific segments of the rRNA (21–26). Methylation is carried out by the action of the methyltransferase Nop1 (fibrillarin in humans) as part of a small nucleolar ribonucleoprotein complex (snoRNP). In this complex, four core proteins (Snu13, Nop56, Nop58, and Nop1) assemble on a snoRNA in a stepwise manner (27). This evolutionarily conserved assembly process requires the action of several assembly factors that confer tight regulation of biogenesis and turnover of box C/D snoRNAs.

Recent quantitative studies have shown that 2′-*O*-methylations are not ubiquitously present on all of the cellular ribosomes, suggesting that these modifications may be an adjustable feature to fine-tune the function of ribosomes (4, 28–36). However, because most rRNA 2′-*O*-methylations are deposited at an early stage during ribosome biogenesis, it is not clear how these modifications can be adjusted or removed, and the source

Significance

The presence of RNA chemical modifications has long been known, but their precise molecular consequences remain unknown. 2′-*O*-methylation is an abundant modification that exists in RNA in all domains of life. Ribosomal RNA (rRNA) represents a functionally important RNA that is heavily modified by 2′-*O*-methylations. Although abundant at functionally important regions of the rRNA, the contribution of 2′-*O*-methylations to ribosome activities is unknown. By establishing a method to disturb rRNA 2′-*O*-methylation patterns, we show that rRNA 2′-*O*-methylations affect the function and fidelity of the ribosome and change the balance between different ribosome conformational states. Our work links 2′-*O*-methylation to ribosome dynamics and defines a set of critical rRNA 2′-*O*-methylations required for ribosome biogenesis and others that are dispensable.

of rRNA 2′-O-methylation heterogeneity remains unknown (4, 5, 37). Attempts to investigate the repertoire of substoichiometric 2′-O-methylation sites of rRNA include the study of natural variations between cell lines (32, 36), changes of rRNA 2′-O-methylations in primary human breast tumors (38), differential rRNA modifications during mouse development (39), changes of modifications in the presence or absence of the antitumor protein p53 (29, 35), which regulates the methyltransferase fibrillarin (40), changes caused by depletion of fibrillarin (28) and RNA helicase Dbp3 (41), and the use of a Nop1 mutant (42). Surprisingly, however, the methods used to study the effect of rRNA hypo-2′-O-methylation have not allowed identification of all potential variable modification sites. For example, mutating the active site of Nop1, which is expected to directly affect rRNA 2′-O-methylations, did not change the methylation pattern of the ribosome (42). The alternative approach of knocking down fibrillarin using small interfering RNA in human cell lines (28), allowed researchers to identify a set of 2′-O-methylations that are specifically reduced in the presence of limiting amounts of fibrillarin. However, because cells depleted of fibrillarin hardly divide or make any new ribosomes and likely rely on their already assembled ribosomes for survival (43–46), limited modification changes were observed using this strategy. Furthermore, which effects of fibrillarin knockdown are direct versus indirect was not discerned (47). Therefore, obtaining a comprehensive view of the rRNA sites that have the potential to be missed, removed, or regulated has not been possible thus far.

To overcome this limitation, we present here a strategy that involves decreasing the biogenesis of box C/D snoRNAs via a single mutation in an essential box C/D snoRNP assembly factor, Bcd1. Bcd1 is an evolutionarily conserved protein that cooperates with several other assembly factors to direct the assembly of box C/D snoRNAs into functional snoRNP complexes (27). Bcd1 controls the steady-state levels of box C/D snoRNAs by regulating the assembly of the Nop58 protein into pre-snoRNPs and by mediating the interaction of Snu13 with snoRNAs (48–50). Using a variant of Bcd1 (*bcd1-D72A*), which causes a global box C/D snoRNA down-regulation but allows cell growth and ribosome biogenesis (50), here, we reveal a wide spectrum of variable rRNA 2′-O-methylation sites in yeast ribosomes and identify their impact on translation. Strikingly, our data reveal that more than 70% of yeast rRNA 2′-O-methylation sites have the potential to be significantly hypo-2′-O-methylated. We also show that 2′-O-methylation affects the dynamics of the rRNA, resulting in a change in the balance between different conformational states of the ribosomes required for translation. Finally, our data show that rRNA hypomethylation also impacts the binding of eukaryotic translation initiation factor 1 (eIF1) to the small ribosomal subunit. Together, these results allow us to dissect those rRNA 2′-O-methylation sites that are critical for ribosome biogenesis from those that are dispensable and may have other functional roles and link rRNA 2′-O-methylation to specific features of the ribosomes.

Results

Heterogeneity of rRNA 2′-O-Methylation Sites in Yeast rRNA Reveals Sites That Are Dispensable for Ribosome Biogenesis. To address which of the rRNA 2′-O-methylations sites are tunable in yeast and identify those that are dispensable for ribosome production in viable cells, we exploited a mutation in the modification machinery that alters the biogenesis of box C/D snoRNPs in actively growing yeast cells. For this purpose, we engineered the *bcd1-D72A* mutation in yeast cells using CRISPR/Cas9 genome editing (50). The introduction of this mutation into the genome ensures that all the ribosomes will be made in the presence of defective Bcd1, which causes cells to have low steady-state levels of box C/D snoRNAs (50). We then performed RiboMethSeq analysis (32) on RNAs isolated from actively growing wild-type control yeast cells and those expressing *bcd1-D72A*. *SI Appendix*, Fig. S1 shows the average MethScores (ScoreC) for all rRNA methylation sites in wild-type control and mutant *bcd1-D72A* cells. In line with the previous observations (31, 32), 47 of the 53 2′-O-methylation sites in wild-type control yeast cells are methylated at high levels (with a MethScore of >0.8), and only a small fraction (6/53 sites) show MethScores below 0.8 (*SI Appendix*, Fig. S1). While the average MethScore for wild-type control is 0.85, analysis of data from *bcd1-D72A* cells revealed a much lower level of methylation (average MethScore of 0.43). These data indicate that the majority of rRNA 2′-O-methylation positions are hypomethylated in *bcd1-D72A* cells.

Analysis of the 2′-O-methylation sites in the 18S rRNA of *bcd1-D72A* cells revealed seven stable sites with similar methylation levels as the wild-type control (MethScore > 0.8), eight variable sites (MethScore between 0.4 and 0.8), and three highly hypomethylated sites (MethScore < 0.4) (Fig. 1A). The decoding center harbors stable modification sites (G1428 and C1639) (Fig. 1 B and C). In contrast, the hypo 2′-O-methylated sites within 18S rRNA do not cluster at a specific region within the 40S subunit. For 25S rRNA, we identified 6 stable sites with near-complete methylation, 15 variable sites, and 14 hypo-2′-O-methylated sites (Fig. 1D). With the exception of two stable modification sites (U2921 and C2959), the peptidyl transferase center (PTC) and the transfer RNA (tRNA) accommodation corridor are devoid of 2′-O-methylated sites. However, several hypo-2′-O-methylated or variable sites neighbor these functional regions (Fig. 1 E and F).

Comparison of the rRNAs in *BCD1* and *bcd1-D72A* cells by Northern blot using probes against 18S and 25S rRNAs does not reveal the presence of any rRNA processing intermediates (50), suggesting that although different rRNA processing intermediates accumulate in *bcd1-D72A* cells, their amounts are negligible compared to the fully processed mature rRNAs. Thus, RiboMethSeq analysis of the total RNA from *bcd1-D72A* is a good proxy for the 2′-O-methylation levels in the mature ribosomes. To test if hypo-2′-O-methylated rRNAs assembled into functional mature ribosomes and validate the RiboMethSeq data, we tested whether the reduced methylation levels observed in *bcd1-D72A* cells are also present in mature purified ribosomes. To this end, we compared the 2′-O-methylation levels of a randomly selected variable site in each of the ribosomal subunits purified from *BCD1* or *bcd1-D72A* cells by reverse transcription at low concentration of deoxyribonucleotide triphosphates (dNTPs) combined with sequencing gel analysis (*SI Appendix*, Fig. S2 A and B). This analysis shows that the 2′-O-methylation level of A974 in 18S rRNA isolated from purified hypo-2′-O-methylated 40S subunits is 0.4 relative to wild-type ribosomes, which is very similar to the estimated fraction methylated based on the MethScore value of 0.49. Similarly, analysis of fraction methylated at A2280 in 25S by quantification of stops in reverse transcription results in a value of 0.42, which is close to the measured MethScore of 0.39 for this site. Taken together, our RiboMethSeq data reveal that while 24.5% (13/53) of rRNA 2′-O-methylation sites are critical for ribosome biogenesis and function, other rRNA 2′-O-methylations can be variable (43.4%, 23/53) or even dispensable (32.1%, 17/53).
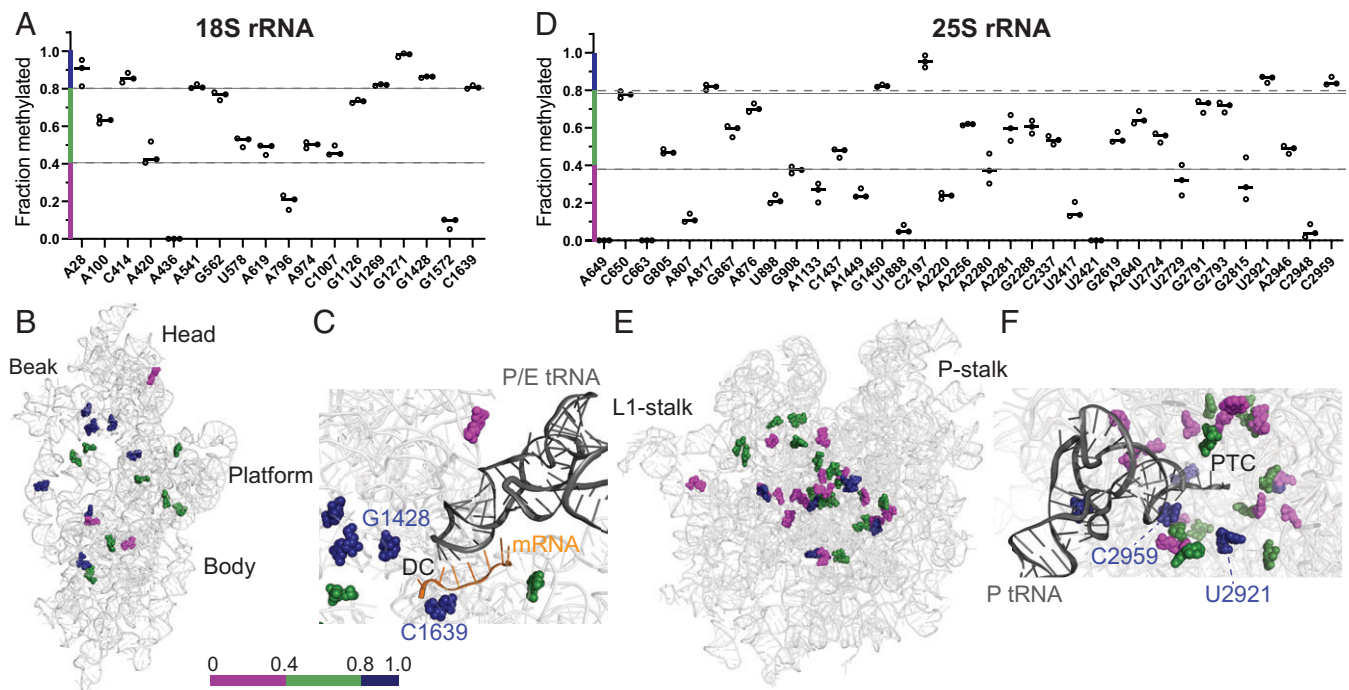
Fig. 1. rRNA 2′-O-methylation sites change in a site-specific manner in *bcd1-D72A* cells. (*A* and *D*) The fraction of 2′-O-methylation (MethScore) at each modification site in 18S (*A*) and 25S (*D*) rRNA in *bcd1-D72A* cells relative to wild-type control cells was evaluated by RiboMethSeq. Data are shown as mean MethScore values for three independent biological replicates. (*B* and *E*) The position of each modification is marked on the 18S (*B*) and 25S (*E*) rRNA structure (Protein Data Bank [PDB] ID: 6GQV). The stable sites (MethScore > 0.8) are colored in blue, the variable sites (0.4 < MethScore < 0.8) are colored in green, and the hypo-2′-O-methylated sites (MethScore < 0.4) are colored in magenta. (*C*) Modifications around the decoding center (DC) within 18S rRNA. (*F*) Modifications around the PTC within 25S rRNA (PDB ID: 4V6I).

rRNA Hypomethylation Affects the Fidelity of Protein Synthesis. rRNA modifications are critically important for the function and fidelity of ribosomes (7, 11, 51, 52). We, therefore, tested whether the change of rRNA 2′-O-methylation pattern in *bcd1-D72A* cells affects the efficiency and accuracy of protein synthesis. To assess the translational efficiency of hypo-2′-O-methylated ribosomes, we analyzed the incorporation rate of L-homopropargylglycine (HPG; an amino acid analog of methionine containing an alkyne moiety that can be fluorescently modified) into newly synthesized peptides in rapidly dividing wild-type or *bcd1-D72A* cells. HPG-containing proteins were fluorescently labeled by the addition of Alexa Fluor 488 and separated from the unincorporated dye by sodium dodecyl sulfate-polyacrylamide gel electrophoresis (SDS-PAGE) (Fig. 2*A*). Quantification of the levels of newly synthesized proteins relative to the total proteins in wild-type and *bcd1-D72A* cells revealed that while total protein synthesis is higher in wild-type control cells, the rate of HPG incorporation over time is not significantly different between the two strains (Fig. 2*B*). However, we observed a higher fluorescent signal at each time point in control cells versus *bcd1-D72A* cells, suggesting a higher number of translating ribosomes in wild-type control cells in agreement with the ribosome biogenesis defects we had previously observed in *bcd1-D72A* cells (50).

To assess the quality of mature ribosomes in *bcd1-D72A* versus wild-type control cells, we analyzed the purified 40S and 60S subunits from both cells by SDS-PAGE and Western blotting. This experiment did not reveal any apparent differences between the protein composition of ribosomes isolated from wild-type and hypo-2′-O-methylated ribosomes (*SI Appendix,* Fig. S2 *C* and *D*).

Because changes in ribosome number and/or composition can affect the accuracy of protein synthesis and impact the

ability of ribosomes to initiate from internal ribosome entry sites (IRESs) (28, 53–55), we next assayed the fidelity of translation in wild-type control and *bcd1-D72A* cells. For this purpose, we used a set of established dual-luciferase reporter plasmids in which the translation of the firefly luciferase depends on a defect in translation fidelity, including −1 and +1 programmed frameshifting, alternate start codon selection, stop codon readthrough, miscoding, or initiation from an IRES element (Fig. 2*C*) (56–60). Cells with lower translation fidelity will have higher expression of the firefly luciferase than control cells. As an internal control, all plasmids contain a constitutively expressed *Renilla* luciferase used for normalization. For each plasmid reporter, the firefly luciferase activity was normalized against *Renilla* activity, and values observed for *bcd1-D72A* cells were normalized against those observed for wild-type control cells. This analysis revealed that, compared to control ribosomes, ribosomes from *bcd1-D72A* cells have an increased rate of near-cognate start codon selection and frameshifting (Fig. 2*D*). The data also revealed that the hypomodified ribosomes have reduced stop codon readthrough as well as IRES-mediated initiation. Thus, translation fidelity and IRES-dependent translation initiation are altered in *bcd1-D72A* cells.

To assess whether the translational defects in *bcd1-D72A* are due to structural changes in ribosomes, we used translation inhibitors that bind to the small (paromomycin and apramycin) or large (homoharringtonine) ribosomal subunits (61) and compared the growth of wild-type control and *bcd1-D72A* cells in liquid medium in the absence or presence of sublethal doses of these drugs. This analysis revealed that *bcd1-D72A* cells are more sensitive than wild-type control cells to the addition of paromomycin and apramycin, aminoglycosides that specifically bind to the small ribosomal subunit at the decoding center. In the presence of these drugs, the fold change in doubling time
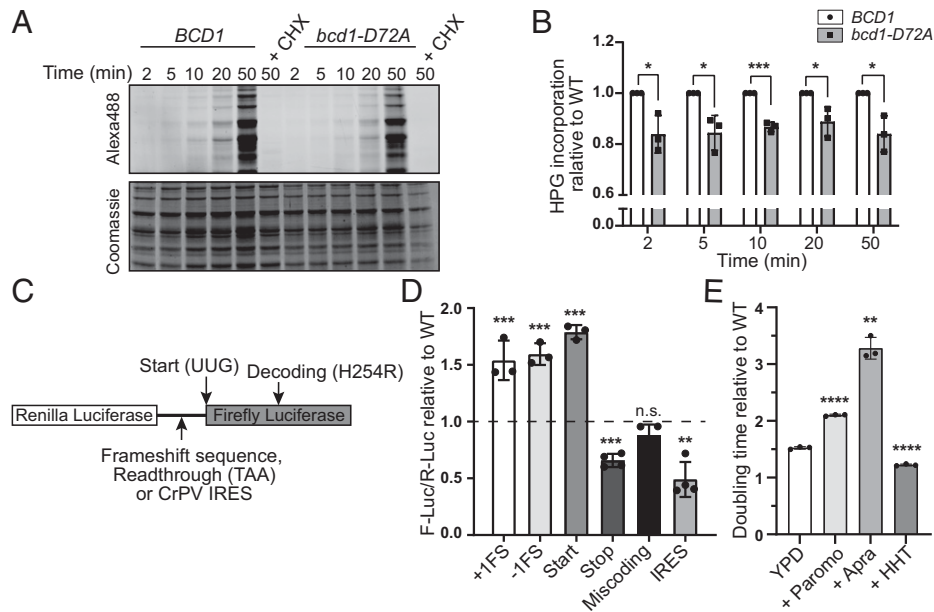
Fig. 2. rRNA hypomethylation affects the function and fidelity of ribosomes. (*A*) Analysis of the incorporation rate of HPG into newly synthesized peptides in rapidly dividing yeast cells expressing wild-type or mutant Bcd1 over a time course (2 to 50 min). HPG-containing proteins were fluorescently labeled by addition of Alexa Fluor 488 and separated from unincorporated dye by SDS-PAGE and imaged (*Top*) before staining with Coomassie blue for total protein detection (*Bottom*). CHX stands for cycloheximide. (*B*) Quantification of the data shown in *A*. At each time point, the ratio of the newly synthesized protein to the total protein for *bcd1-D72A* cells is normalized to the wild-type cells. Three biological replicates were analyzed. (*C*) Schematic of the dual-luciferase plasmids used in this study. For all plasmids, *Renilla* luciferase is constitutively expressed, while the expression of firefly luciferase is dependent on a specific translational defect/element. (*D*) Expression of firefly and *Renilla* luciferase was measured in wild-type control or *bcd1-D72A* yeast harboring the indicated plasmids. The ratio of firefly luciferase to *Renilla* luciferase was normalized to the control plasmids and shown relative to wild type; three to four biological replicates were analyzed. (*E*) Doubling times of wild-type control and *bcd1-D72A* cells were measured in medium with or without translational inhibitors. The fold change, calculated by dividing the doubling time values of *bcd1-D72A* cells to wild-type control cells in each condition, is plotted. Three biological replicates were analyzed. In *B*, *D*, and *E*, column bars represent the mean values, and the error bars depict the SDs; Paromo, paromomycin; Apra, apramycin; HHT, homoharringtonine. Significance was determined using a *t* test; *$P \leq 0.05$; **$P \leq 0.01$; ***$P \leq 0.001$; ****$P \leq 0.0001$; n.s., nonsignificant.

of *bcd1-D72A* cells relative to wild-type control cells significantly increases (Fig. 2*E*). In contrast, *bcd1-D72A* cells are hyposensitive to homoharringtonine, which binds in the large ribosomal subunit tRNA A site (Fig. 2*E*). These data suggest structural changes in both the small and large ribosomal subunits that can affect the binding between ribosome and ligands, such as translational inhibitors, tRNAs, or IRES elements.

rRNA Hypo-2′-*O*-Methylation Impacts the Rotational Status of Ribosomes. Recent work has shown that messenger RNA (mRNA) structures that promote programmed frameshifting in bacteria change the reading frame of the ribosome by increasing the rotated-state pause (62–64), thus providing a link between ribosome dynamics and frameshifting. A pseudoknot in severe acute respiratory syndrome coronavirus 2 mRNA also causes translation pausing prior to −1 frameshifting in mammalian ribosomes by providing a bulky and well-structured obstacle wedged at the mRNA entry channel (65). Because 2′-*O*-methylation affects the flexibility of RNA, we hypothesized that the observed changes in mRNA frameshifting in *bcd1-D72A* cells could arise from altered dynamics of the ribosome. To address this question, we used RNA structure probing. Several key residues in both the small and large ribosomal subunits undergo detectable changes in conformation upon transition between rotated and nonrotated ribosomal states (66). The most prominent of these sites is G913 in 18S rRNA (SSU-G913), which is located at the intersubunit bridge B7a. To compare the rotational dynamics of the wild-type control and hypomethylated ribosomes, we probed this nucleotide in wild-type and *bcd1-D72A* cells using phenylglyoxal (PGO) (Fig. 3*A*). As a reference, we took advantage of two mutations in *RPL3* (*rpl3-W255C* and *rpl3-H256A*) that

are known to stabilize ribosomes in nonrotated and rotated states, respectively (67). We then compared the rotational status of wild-type and hypo-2′-*O*-methylated ribosomes to the rotated and nonrotated ribosomes from *RPL3*-mutant cells (Fig. 3*B*).

Our analyses reveal that in vivo, the SSU-G913 nucleotide in *rpl3-W255C* ribosomes is protected and shows minor reactivity to PGO. In *rpl3-H256A* cells, however, in which the ribosomes are stabilized in the rotated state, the SSU-G913 nucleotide is more accessible when probed with PGO. Comparing the reactivity of SSU-G913 in wild-type control and *bcd1-D72A* cells with those of *rpl3-W255C* and *rpl3-H256A* revealed that the hypomethylated ribosomes from *bcd1-D72A* cells are at least as accessible to PGO as the rotated ribosomes from *rpl3-H256A* cells, suggesting that the majority of ribosomes from *bcd1-D72A* cells are in the rotated conformation relative to the wild-type control (Fig. 3 *A* and *B*). These data suggest that ribosomes from *bcd1-D72A* cells favor the rotated state and that the increased rate of frameshifting in hypomethylated ribosomes could be due to the increased time the hypo-2′-*O*-methylated ribosomes spend in the rotated state.

Elongation factor 2 (EF-G in bacteria and eEF2 in eukaryotes) binds to pretranslocation ribosomes and stabilizes the rotated state (68). Mutations in yeast ribosomes that stabilize the rotated conformation increase the affinity of eEF2 for ribosomes (66, 67). Overexpression of eEF2 causes stabilization of the rotated ribosomes by mass action and impairs yeast growth (Fig. 3 *C* and *D*). Therefore, we hypothesized that as the hypo-2′-*O*-methylated ribosomes preferentially assume the rotated conformation in the cell, the overexpression of eEF2 should have less deleterious effects on *bcd1-D72A* cells than on wild-type controls. To test this, we compared the growth of wild-type control and
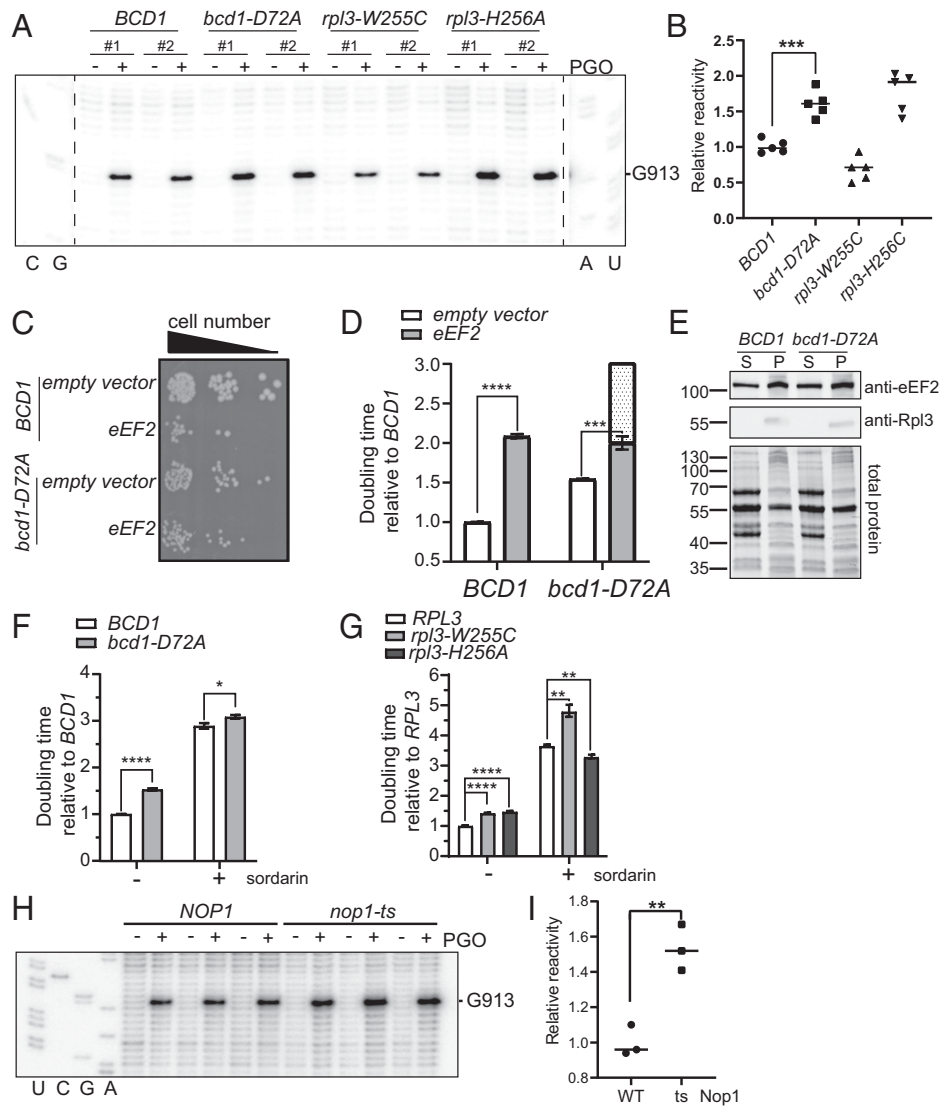
Fig. 3. Hypo-2′-O-methylated ribosomes adopt a more rotated conformation in vivo. (*A*) In vivo RNA structure probing of cells expressing either wild-type or the D72A variant of Bcd1 with or without PGO treatment to probe the accessibility of SSU-G913. Cells expressing W255C or H256A variants of Rpl3 were used as controls for rotation status. Two biological replicates are shown in the figure. (*B*) Quantification of the SSU-G913 modification by PGO. Five biological replicates were analyzed. (*C*) *bcd1-D72A* cells are less sensitive to the overexpression of eEF2 than wild-type cells. Indicated cells were serially diluted on selective plates and grown for 48 h at 30 °C. (*D*) Quantification of the growth of *BCD1* and *bcd1-D72A* cells expressing eEF2. The dot pattern indicates the expected doubling time of *bcd1-D72A* cells if there was no rescue of eEF2 overexpression by the *bcd1-D72A* mutation. (*E*) Western blot against free (S, supernatant) and ribosome-bound (P, pellet) eEF2 from formaldehyde-fixed whole-cell extracts from *BCD1* or *bcd1-D72A* cells separated by centrifugation over a sucrose cushion. Rpl3 serves as an indicator of ribosome pelleting. (*F*) *bcd1-D72A* cells are less sensitive to sordarin (3 μg/mL) than wild-type cells. (*G*) Whereas *rpl3-W255C* cells have the same sensitivity to sordarin as the wild-type cells, *rpl3-H256A* shows less sensitivity to sordarin. In *D, F,* and *G,* four biological replicates were analyzed. (*H*) Probing the accessibility of SSU-G913 in *NOP1* and *nop1-ts* using PGO. Three biological replicates are shown in the figure. (*I*) Quantification of the SSU-G913 modification by PGO. In *B, D, F, G,* and *I,* bars represent the mean values. The error bars in *D, F,* and *G* depict the SDs. Significance for all graphs was analyzed using a *t* test; *P ≤ 0.05; **P ≤ 0.01; ***P ≤ 0.001; ****P ≤ 0.0001.

bcd1-D72A yeast cells overexpressing eEF2 on solid medium. While overexpression of eEF2 causes a severe growth defect in wild-type cells, as evident from the smaller colony size, it does not impact the growth of *bcd1-D72A* cells to the same extent (Fig. 3*C*). To further quantify this growth difference, we measured the growth of wild-type control and *bcd1-D72A* yeast cells overexpressing eEF2 during their logarithmic phase of growth. The *bcd1-D72A* cells grow slower than wild-type control cells by 1.3- to 1.5-fold depending on the plasmid they harbor and the medium they are growing in. We observed that *bcd1-D72A* cells overexpressing eEF2 grow slower than *bcd1-D72A* cells harboring the empty vector (Fig. 3*D*). However, because ribosomes in *bcd1-D72A* cells have a conformational bias toward the rotated state, these cells are affected to a lesser extent than wild-type control cells by overexpression of eEF2. These data indicate that

bcd1-D72A cells are less sensitive to the overexpression of eEF2 than the control cells (Fig. 3*D*). An alternative explanation is that reduced sensitivity of the *bcd1-D72A* strain to eEF2 overexpression is due to a reduction of eEF2–ribosome affinity. To test this, we compared the binding of eEF2 to the ribosomes in vivo. To this end, *bcd1-D72A* and wild-type control cells were grown to mid-log phase and fixed with formaldehyde. The ribosome-bound and free eEF2 were then separated by centrifugation through a sucrose cushion. As shown in Fig. 3*E,* we do not observe any difference between the ribosome-bound eEF2 fraction in *bcd1-D72A* and control cells. Thus, the lower sensitivity of *bcd1-D72A* cells to eEF2 overexpression is unlikely to be due to the reduced affinity of eEF2 for hypomethylated ribosomes.

To further test whether hypomethylated ribosomes spend more time in the rotated state, we measured the growth of

bcd1-D72A and control cells in the presence of sordarin. Sordarin is an inhibitor of eEF2 that binds to ribosome-bound eEF2 and prevents its domain movements, which are required for translocation (69). We analyzed the effect of sordarin on the growth of *bcd1-D72A* and wild-type control cells and compared that to the growth of reference cells expressing wild-type *RPL3*, *rpl3-W255C*, or *rpl3-H256A*. Whereas cells expressing wild-type *RPL3* and *rpl3-W255C* show similar sensitivity to sordarin, *rpl3-H256A* and *bcd1-D72A* cells are both less sensitive to sordarin (Fig. 3 *F* and *G*). These data further support the notion that hypo-2′-*O*-methylated ribosomes, similar to *rpl3-H256A*–harboring ribosomes, spend more time in the rotated state. Taken together, these data provide evidence that the 2′-*O*-methylation status of rRNA affects the ribosomal rotation state. Importantly, because there are no 2′-*O*-methylation sites near the SSU-G913 nucleotide, our data suggest that the ribosome rotational changes observed in *bcd1-D72A* cells are due to long-range effects.

Recent studies have proposed a function for snoRNAs in chaperoning the folding of rRNA (70). The levels of box C/D snoRNAs are significantly lower in *bcd1-D72A* cells than in wild-type control cells (48, 50). The changes we detected in the conformation of ribosomes could therefore arise either directly from the lack of 2′-*O*-methylations or indirectly from the decreased levels of snoRNAs. To dissect the role of snoRNA binding and chaperoning from the effect of rRNA 2′-*O*-methylations on the ribosome structure, we took advantage of a temperature-sensitive (ts) mutation in the methyltransferase Nop1 (71). Cells harboring this mutation grew more slowly than wild-type control cells at 37 °C and had lower rRNA methylation levels but did not show any change in snoRNA levels (*SI Appendix*, Fig. S3). In vivo analysis of the SSU-G913 modification by PGO in *nop1-ts* cells compared to wild-type control cells showed higher accessibility of SSU-G913 in *nop1-ts* cells, suggesting stabilization of the rotated ribosomal conformation in the hypo-2′-*O*-methylated ribosomes (Fig. 3 *H* and *I*). Because the level of snoRNAs is similar to the wild-type control cells in the *nop1-ts* cells, these data indicate that the observed defects in the inherent dynamics of the ribosome in *bcd1-D72A* cells are more due to the decreased rRNA 2′-*O*-methylation rather than a decrease in snoRNA levels.

Binding of eIF1 to the Hypo-2′-*O*-Methylated Small Ribosomal Subunit Is Weakened In Vivo and In Vitro. eIF1 plays an important role in ensuring the selection of the cognate start codon and antagonizing the near-cognate start codon selection by stabilizing the open, scanning-competent conformation of the small ribosomal subunit (40S) (72–74). Upon proper start codon selection, eIF1 is released from 40S, allowing rearrangement of the ribosome from the open to closed conformation (57, 75). Because ribosomes from *bcd1-D72A* cells show an elevated level of near-cognate start codon recognition (Fig. 2*D*), we hypothesized that the hypo-2′-*O*-methylated ribosomes from *bcd1-D72A* cells cannot bind to eIF1 as efficiently as wild-type ribosomes. To test this hypothesis, cells expressing wild-type or the D72A variant of Bcd1 were fixed with formaldehyde in the mid-log phase, and ribosome-bound and free eIF1 were separated by centrifugation on sucrose density gradients and quantified by Western blotting. While ~25% of eIF1 comigrates with the ribosomes in wild-type control cells, the binding of eIF1 to the hypo-2′-*O*-methylated ribosomes in *bcd1-D72A* cells is significantly reduced (Fig. 4*A*).

To corroborate this finding, we next assessed the binding of eIF1 to 40S ribosomal subunits isolated from wild-type control

and *bcd1-D72A* cells. For this purpose, we fluorescently labeled eIF1 at its N terminus and determined its binding affinity for purified 40S subunits using a temperature-related intensity change assay. Notably, the N terminus of eIF1 is located away from the 40S and therefore is unlikely to be affected by possible changes in the ribosome conformation around its binding site (*SI Appendix*, Fig. S4A). The results from these binding assays revealed that eIF1 binds to 40S subunits isolated from wild-type cells with a dissociation constant (K_d) of ~20 nM, comparable to previous reports (76). However, the affinity of eIF1 for hypo-2′-*O*-methylated 40S ribosomal subunits was lower by threefold (~60 nM) (Fig. 4*B*). In line with this decrease in affinity, overexpression of eIF1, but not eIF1A, rescues the growth defects in *bcd1-D72A* cells to a great extent, while it does not affect the wild-type control cells (Fig. 4*C*).

The biochemical and genetic data above suggest that rRNA 2′-*O*-methylations play a key role in regulating the binding of eIF1, thereby ensuring the stringency of start codon selection. A prediction from this finding is that other factors/mutants that antagonize the near-cognate start codon selection could at least partially rescue the slow growth phenotype of *bcd1-D72A* cells. To test this idea, we took advantage of two *rps3* missense mutants (R116D and R117D) that destabilize the closed conformation of the 48S preinitiation complex (PIC) and antagonize the near-cognate start codon selection (77). We replaced the endogenous promoter of the *RPS3* gene with a galactose-inducible/glucose-repressible promoter in wild-type control and *bcd1-D72A* cells. This allowed us to compare the impact of expression of wild-type and mutant versions of *RPS3* on the growth of wild-type control and *bcd1-D72A* cells by transforming in plasmids encoding these variants and turning off the expression of endogenous *RPS3*. Interestingly, expression of both variants of *RPS3* rescued the slow growth defect of *bcd1-D72A* cells (Fig. 4*D*).

The 18S rRNA folds into distinct domains known as head, shoulder, and body (*SI Appendix*, Fig. S5). The mRNA-binding site lies within a cleft between the head and body domains. In the open, scanning-competent conformation, the head and body domains are farther apart from each other than in the closed conformation, allowing for rapid movement of the 40S on the mRNA. In the closed conformation, the head and body come close to each other, locking the initiation codon in the P site (78, 79). A distinct structural feature of the closed state is the appearance of the mRNA latch composed of elements in h18 in the body with h34 and Rps3 in the head domain (73). Comparing the latch nucleotides in the closed and open conformations (80) suggests that the A579 nucleotide is more solvent accessible in the open conformation and hence more likely to be modified by RNA structure–probing reagents (*SI Appendix*, Fig. S5). To probe if the equilibrium between the open and closed conformations of 40S is affected in hypo-2′-*O*-methylated ribosomes, we treated 40S subunits isolated from control or *bcd1-D72A* cells with dimethyl sulfate (DMS) and analyzed the accessibility of the A579 nucleotide (Fig. 4*E*). Our analysis shows a decreased reactivity of the A579 nucleotide toward DMS in *bcd1-D72A* cells relative to the control cells, suggesting that the mRNA latch is closed in a higher population of 40S ribosomes in *bcd1-D72A* than in wild-type control cells (Fig. 4*F*).

Altogether, these data strongly suggest that rRNA hypo-2′-*O*-methylation changes the inherent conformational dynamics of ribosomes, thereby impacting ribosome–factor interactions, leading to translational errors. Thus, the deficiency in start codon selection in hypo-2′-*O*-methylated ribosomes may be
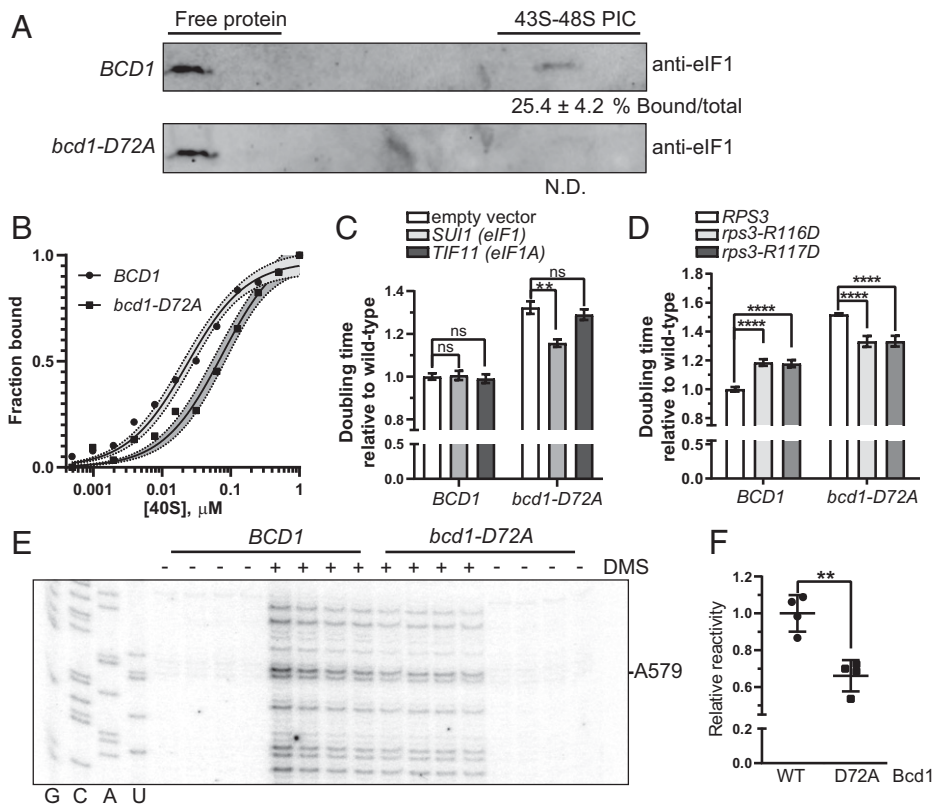
Fig. 4. Binding of eIF1 to hypomethylated 40S is weakened in vivo and in vitro. (*A*) Western blot against eIF1 for the fractions of sucrose gradients of formaldehyde-fixed whole-cell extracts from *BCD1* (*Top*) or *bcd1-D72A* (*Bottom*) cells. The ratio of eIF1 in 43S–48S PIC relative to the total eIF1 is depicted under each blot. Two biological replicates were analyzed. N.D. stands for not determined. (*B*) Fraction of eIF1 bound to 40S plotted against the 40S concentration. Data were fitted with a nonlinear regression model in GraphPad Prism 8.0 to yield dissociation constants of 23 nM and 64 nM for wild-type and hypo-2′-*O*-methylated ribosomes, respectively; 95% confidence levels are shown in shades of gray. (*C*) Comparison of doubling times of *BCD1* and *bcd1-D72A* cells harboring either an empty vector or vectors expressing *SUI1* (eIF1) or *TIF11* (eIF1A) in minimal medium containing glucose. Four biological replicates were analyzed. (*D*) Comparison of doubling times of *BCD1* and *bcd1-D72A* cells in which the endogenous Rps3 is depleted and either wild-type or R116D or R117D variants of Rps3 are expressed from a plasmid. Four biological replicates were analyzed. (*E*) Probing the accessibility of SSU A579 in 40S ribosomal subunits purified from *BCD1* and *bcd1-D72A* cells using DMS. Four biological replicates are shown in the figure. (*F*) Quantification of data shown in *E* for the SSU A579 modification by DMS. In *C*, *D*, and *F*, bars represent the mean values, and the error bars depict the SDs. Significance was analyzed using a *t* test. n.s., nonsignificant; ** $P \leq 0.01$; ****$P \leq 0.0001$.

attributed to the weaker binding of the ribosome to eIF1 and changes in ribosome dynamics.

Discussion

snoRNA-guided ribose 2′-*O*-methylation is an evolutionarily conserved common form of methylation in rRNA. Even though RNA 2′-*O*-methylation changes have been linked to a large number of human diseases (5, 8, 38, 40, 55, 81, 82), the role of rRNA 2′-*O*-methylations for the function of ribosomes is not understood to date. Recent findings indicate the plasticity of 2′-*O*-methylation in rRNA, proposing avenues for fine-tuning the function of the ribosome (5, 28, 29, 36, 38, 39). Here, we describe a strategy for surveying the repertoire of substoichiometric rRNA 2′-*O*-methylation sites by exploiting a defect in box C/D snoRNP assembly. This approach allowed us to lower the overall level of box C/D snoRNAs, thereby globally changing rRNA 2′-*O*-methylations without severely affecting cell survival, enabling us to probe rRNA 2′-*O*-methylation changes that had remained elusive so far.

Interestingly, as suggested from previous studies of human snoRNAs (29), comparing the snoRNA levels to the fraction of modification of their corresponding 2′-*O*-methylation sites indicated that there was no direct correlation between the steady-state box C/D snoRNA levels and the methylation status of nucleotides. While the majority of box C/D snoRNA levels

decreased by more than 60% in *bcd1-D72A* cells, in some cases, we observed near-complete 2′-*O*-methylation (*SI Appendix,* Table S1). The observation that most stable methylation sites had their corresponding snoRNA levels reduced by 80 to 90% suggests a threshold model for rRNA modification where the presence of even a small amount of snoRNAs is sufficient for 2′-*O*-methylation of the majority of transcribed rRNA.

Of the 53 2′-*O*-methylation sites in yeast rRNA, 38 are conserved between yeast and humans. The potential of these conserved sites for variability in their methylation was assessed previously after knockdown of the methyltransferase fibrillarin (28). This study showed that 6/38 of the conserved sites between yeast and humans were less than 80% methylated and could be substantially altered. With our approach of manipulating snoRNA levels in yeast, we identified 25/38 conserved sites in yeast that were methylated in less than 80% of the rRNA population (*SI Appendix,* Fig. S6). Interestingly, all but one of the six variable conserved sites that were identified in human rRNA had their yeast equivalents also hypomodified in the *bcd1-D72A* mutants. The Cm2197 site in yeast rRNA is the only exception that remains fully methylated in *bcd1-D72A* cells, yet its human equivalent shows significant hypomethylation in fibrillarin-depleted HeLa cells (28). We attribute this difference to the resistance of the guiding snoRNA, snR76, to *bcd1-D72A* mutation (*SI Appendix,* Table S1) or the higher stability of this snoRNA. A possible explanation for the higher

number of variable modifications in yeast rRNA than in human rRNA could result from organismal differences. However, as opposed to cells depleted of fibrillarin, which undergo limited division and do not make new ribosomes, the *bcd1-D72A* yeast cells we have used in this study keep dividing and making new ribosomes (50). This can result in a higher rate of hypomodification and allow us to map substoichiometric 2′-*O*-methylations in a more thorough way than was possible previously.

While most of the box C/D snoRNAs in yeast guide the site-specific modification of rRNA, a few snoRNAs play a role in rRNA folding and processing (83). Recently, the box H/ACA snR35 was proposed to prevent the premature folding of helix 31 in pre-40S, thereby contributing to rRNA folding in a manner distinct from its modifying role (70). Given the decrease in snoRNA levels in *bcd1-D72A* cells relative to wild-type control cells, we tested whether the changes in the dynamics of the ribosomes arise from the lack of methylation or decreased snoRNA levels. Our results show that altered inherent ribosomal dynamics can be caused by changes in rRNA 2′-*O*-methylation but not by the loss of snoRNAs and their chaperoning effect. These findings corroborate previous work on several box C/D and H/ACA snoRNAs, which point to the importance of rRNA modifications in addition to the chaperoning role of snoRNAs (52). However, further studies are required to dissect the potential role of snoRNAs in chaperoning rRNA folding and investigating the contributions from these events to rRNA dynamics.

Whereas deletion of most individual box C/D snoRNAs does not have a major effect on yeast cell growth under normal conditions (84–86), simultaneous deletion of groups of rRNA 2′-*O*-methylations or using a ts Nop1 severely affects cell growth and results in translation defects (4, 44, 87). For example, the absence of modifications in 25S H69 as well as around the decoding center and the A-site finger causes translational errors, including stop codon readthrough, +1 frameshifting, and −1 frameshifting (51, 87). Mapping 2′-*O*-methylation changes arising from fibrillarin knockdown onto the ribosome structure revealed that altered 2′-*O*-methylations can be found in several regions involved in intermolecular interactions, such as between tRNA and the A site, intersubunit bridges, or around the peptide exit tunnel (28). While these changes in 2′-*O*-methylation levels did not affect translation elongation, they affected the IRES-mediated translation initiation.

Our data reveal that changes in 2′-*O*-methylation levels can affect translation fidelity in multiple ways. In addition to modulating IRES-dependent translation initiation, similar to what was observed after fibrillarin knockdown, we also observed an increase in the rate of frameshifting and near-cognate start codon recognition. Frameshifting involves the pause of the ribosomal subunits in the rotated state prior to translocation (62–64). Our data indicate that hypo-2′-*O*-methylated ribosomes from *bcd1-D72A* cells favor the rotated state in vivo (Fig. 3 *A–G*). Because we observe a similar preference in rotational state of ribosomes in Nop1-deficient cells (Fig. 3 *H* and *I*), our data suggest that the observed changes in rRNA dynamics are mainly due to the alteration of rRNA 2′-*O*-methylation pattern and not the rRNA folding defects resulting from the reduced snoRNA levels.

Previously, global pseudouridylation defects were shown to affect the binding of the A- and P-site tRNAs to the ribosome, explaining the increased frameshifting and decreased stop codon readthrough rates of such ribosomes (11). Mapping of the hypomethylation sites around the E- and P-site tRNAs did not reveal dramatic changes in the methylation pattern, with the exception of two sites near the acceptor arm of each tRNA (*SI Appendix*, Fig. S4 *B* and *C*). We also did not observe a change in the rate of HPG incorporation into newly synthesized proteins despite its overall lower incorporation at any time point (Fig. 2*A*), suggesting that the translation rate remains unchanged. These findings corroborate the previous observation that hypo-2′-*O*-methylation does not affect the elongation rate (28). Whether long-range effects from hypo-2′-*O*-methylated sites can also influence tRNA binding remains to be addressed.

To our knowledge, the effect of rRNA 2′-*O*-methylations on the near-cognate start codon selection was unknown to date. Here, we show that eIF1, a major antagonist of near-cognate start site selection, has a lower affinity for hypo-2′-*O*-methylated 40S than wild-type 40S (Fig. 4 *A* and *B*). Interestingly, overexpression of eIF1, but not eIF1A, substantially suppresses the slow growth phenotype of *bcd1-D72A* cells without affecting the growth of wild-type control cells (Fig. 4*C*). A point mutation in the *RPS3* gene, which hampers the near-cognate start codon selection, also substantially rescues the slow growth phenotype of *bcd1-D72A* cells (Fig. 4*D*). Collectively, these results suggest that a major role of 2′-*O*-methylation of ribosomes is to support faithful translation initiation. The increased rate of near-cognate start site selection results in the production of peptides from many short open reading frames (88) or the production of proteins with extended N termini (89). Recently, near-cognate start site selection was also linked to the redistribution of many proteins from the cytosol to mitochondria due to the gain of N-terminal mitochondrial-targeting signals (90). It is not yet clear whether rRNA hypo-2′-*O*-methylation causes similar defects.

Based on the binding data presented, the eIF1 affinities for wild-type and hypomethylated ribosomes are 23 and 63 nM, respectively (Fig. 4*B*). The observed threefold reduction in the eIF1 affinity for ribosomes would not significantly reduce the fractional saturation of the binding interaction at physiological cellular concentrations of eIF1 (91). While the affinity of eIF1 for the wild-type 40S is very high, its affinity for the mRNA-bound 43S PIC is much lower (5- to 20-fold, depending on the nature of the P-site codon) (57). Therefore, we speculate that a threefold reduction in the binding affinity of eIF1 to hypo-2′-*O*-methylated 40S compared to the wild-type would significantly reduce the interaction of eIF1 with the mRNA-bound 40S at physiological cellular concentrations of eIF1 (91).

We noticed that, based on the accessibility of the nucleotide A579 of the mRNA latch, vacant hypo-2′-*O*-methylated 40S subunits assume a more closed conformation than the control ribosomes (Fig. 4 *E* and *F*). As we did not detect major changes in the 2′-*O*-methylation of rRNA in the vicinity of the eIF1-binding site (*SI Appendix*, Fig. S4*A*), we speculate that the decreased affinity of eIF1 for the ribosome is due to a change in the dynamics of the 40S ribosomal subunit (92). According to this model, in vacant 40S, the head and body fluctuate relative to each other, and eIF1 preferentially binds and stabilizes the open conformation. In *bcd1-D72A* cells, the equilibrium between open and closed conformations is altered (Fig. 4 *E* and *F*), resulting in weaker binding of eIF1 to the 40S subunit. Future studies are needed to test this model.

Materials and Methods

Plasmids and Strains. Plasmids used in this study are listed in *SI Appendix*, Table S2. All mutations were introduced by site-directed mutagenesis and confirmed by sequencing. Strains are listed in *SI Appendix*, Table S3. All yeast

strains were confirmed by PCR followed by sequencing as well as Western blotting when antibodies were available.

RiboMethSeq. RiboMethSeq was essentially performed as previously reported (32). Briefly, 150 ng of total RNA was fragmented under denaturing conditions using an alkaline buffer (pH 9.4) to obtain an average size of 20 to 40 nucleotides. Fragments were end repaired and ligated to adapters using a NEBNext Small RNA kit for Illumina. Sequencing was performed on an Illumina HiSeq1000. Reads were mapped to the yeast rDNA and snoRNA sequences, and the MethScore (fraction methylated) was calculated as MethScore (for ± 2 nucleotides) (93), equivalent to "ScoreC" in Birkedal et al. (31). Statistical significance was determined by Student's t test ($P < 0.05$).

HPG Incorporation Assay. BY4741 and *bcd1-D72A* cells were transformed with pRS411 and grown in synthetic medium lacking methionine at 30 °C to mid-log phase. HPG was added to 10-mL cultures to a final concentration of 50 μM, and cells were incubated at 30 °C. At each indicated time point, 2 mL of the culture was removed, and cells were washed with cold water and frozen in liquid nitrogen. The cell pellets were resuspended in 100 μL of lysis buffer (50 mM Tris-HCl, pH 7.4, 150 mM sodium chloride, 1 mM ethylenediamine tetraacetic acid (EDTA), 1 mM ethylene glycol tetraacetic acid (EGTA), 1% Triton X-100, 1% sodium deoxycholate, and 0.1% SDS) supplemented with protease inhibitors, mixed with disruption beads, and lysed in a bead beater. After clearing the lysate, the protein concentration was measured by bicinchoninic acid assay (Thermo Fisher), and an equal amount of protein was used for labeling by Alexa Fluor 488 using the Click-iT HPG Alexa Fluor 488 protein synthesis assay kit (Thermo Fisher). Labeled proteins were resolved on a 12% SDS gel and visualized on a ChemiDoc Imager (Bio-Rad). Total protein was visualized after Coomassie staining and imaged using ChemiDoc.

Fidelity Assay. Translation fidelity was measured using previously established dual-luciferase reporters (56–60). For measurements, 1 mL of BY4741 and *bcd1-D72A* cells expressing the dual-luciferase plasmids were pelleted in the mid-log phase, washed, and frozen in liquid nitrogen. Luciferase activities were measured using the Promega dual-luciferase kit by resuspending cells in 100 μL of 1× passive lysis buffer and incubating for 10 min. The firefly luciferase activity was measured by mixing 10 μL of lysates with 30 μL of Luciferase Assay Reagent II in white, clear-bottom 96-well microplates (Costar). For the same sample, the *Renilla* activity was measured by addition of 30 μL of Stop&Glo reagent. Measurements were performed using a Synergy microplate reader (BioTek). For each sample, firefly luciferase activity was normalized against *Renilla* activity, and then values observed for *bcd1-D72A* were normalized against wild-type control.

In Vivo RNA Structure Probing. BY4741 and *bcd1-D72A* cells were grown to the mid-log phase at 30 °C. SSU-G913 was probed using PGO. The cultures were divided into two tubes, mixed with either PGO (16 mM final concentration) or an equal volume of dimethyl sulfoxide, and incubated for 5 min at 30 °C before washing with water. RNA was extracted using phenol/chloroform and precipitated with ethanol. Precipitated RNA was resuspended in water and treated with DNase I (Bio-Rad) and further purified with the Quick RNA miniprep kit (Zymo Research) before reverse transcription was performed using SuperScript III (Thermo Fisher) according to the manufacturer's protocol. To probe SSU-G913 in *nop1-ts* cells, experimental ts cells and wild-type control cells were grown to mid-log phase at 37 °C before treatment with PGO as before. Data were quantified using Image Lab Software (Bio-Rad). The intensity of bands at the reverse transcription stops were normalized to all band intensities below the stop signal.

In Vitro RNA Structure Probing. Purified 40S ribosomes (25 nM) from control or *bcd1-D72A* cells were mixed with 200 mM DMS or ethanol in 80 mM HEPES/NaOH (pH 7.4), 50 mM NaCl, and 0.5 mM MgOAc. The mixture was incubated at 30 °C for 5 min before quenching with 400 mM β-mercaptoethanol/ 600 mM NaOAc. The RNA was precipitated with ethanol and further purified using a Quick RNA miniprep kit (Zymo Research) before reverse transcription was performed using SuperScript III (Thermo Fisher) according to the manufacturer's protocol. Data were quantified using Image Lab Software (Bio-Rad). To quantify nucleotide accessibility and account for loading differences, the intensity of bands at the reverse transcription stops were normalized to all band intensities below the stop signal.

In Vivo Ribosome Binding Assay. In vivo cross-linking of the translation factors to the ribosome was done as previously described (94). Briefly, cells grown to mid-log phase were chilled by addition of crushed ice (25% of total culture volume) and cross-linked by addition of formaldehyde to a final concentration of 1% relative to the original volume of the culture. After a 1-h incubation in an ice bath, cells were pelleted by centrifugation, washed with chilled water, and resuspended in the lysis buffer (20 mM Tris-HCl, pH 7.5, 100 mM KCl, and 10 mM $MgCl_2$) supplemented with protease inhibitors and RNase inhibitor and frozen in liquid nitrogen. Cells were ruptured by grinding under cryogenic conditions. To monitor eIF1 binding to 40S, the lysate was cleared by centrifugation, and 20 U of optical density at 260 nm (OD_{260}) was loaded on a sucrose gradient (7.5 to 30% sucrose in the lysis buffer) and centrifuged in an SW41 rotor (Beckman Coulter) at 40,000 rpm for 5 h. Gradients were fractionated and analyzed by Western blotting using eIF1 antibody (a gift from A.G. Hinnebusch). To assess the binding of eEF2 to the ribosomes, 20 OD_{260} of cleared lysate was loaded on 100 μL of sucrose cushion (1 M sucrose in lysis buffer) and centrifuged in TLA 100 (Beckman Coulter) for 2 h at $400,000 \times g$. The pellet was resuspended in lysis buffer plus SDS loading dye, and equal volumes of pellet and supernatant were analyzed by Western blotting using antibodies against eEF2 (Kerafast) and Rpl3 (Developmental Studies Hybridoma Bank).

Purification of 40S and eIF1. The 40S ribosomes from BY4741 and BCD1-D72A cells were purified as previously described (95). eIF1 was expressed as a His-tagged protein in Rosetta2(DE3) cells from the pET23-TEV-eIF1 plasmid. Protein expression was induced at an OD_{600} of ∼0.6 by addition of 1 mM isopropyl-β-D-1-thiogalactopyranoside, and the cultures were incubated for 16 h at 18 °C. eIF1 was purified on resin in buffer A (500 mM NaCl, 50 mM HEPES-NaOH pH 7.5, 20 mM imidazole, and 5% glycerol). The protein was eluted with 240 mM imidazole and further purified over a Superdex S-75 gel filtration column (GE Healthcare) equilibrated in 150 mM NaCl, 20 mM HEPES-NaOH pH 7.5, 5% glycerol, and 1 mM dithiothreitol.

eIF1–40S Binding Assay. His–eIF1 was labeled with NT650 fluorophore through noncovalent linkage to the His-tag moiety using the Monolith protein labeling kit RED-Tris-NTA second generation (NanoTemper Technologies). The 40S subunits (0.58 nM to 1.2 μM) isolated from wild-type control or *bcd1-D72A* cells were incubated with 100 nM labeled eIF1. Fluorescence was measured using a Dianthus NT.23 Pico instrument (NanoTemper Technologies). Fluorescence values were baseline corrected, and changes in fluorescence values were used to calculate bound fractions, which were plotted against 40S concentration. Data were fitted with a nonlinear regression model in GraphPad Prism 8.0.

Growth Assay. Cells grown to mid-log phase in minimal medium were diluted into fresh medium, and growth rates were measured in an Epoch2 microplate reader (BioTek) by recording the OD_{600} every 20 min. For growth assays in the presence of translation inhibitors, the following concentrations were used: 500 μg/mL paromomycin, 1 mg/mL apramycin B, 250 μg/mL homoharringtonine, and 3 μg/mL sordarin.

Analysis of the Steady-State Levels of snoRNAs. *NOP1* or *nop1-ts* cells were grown in yeast–peptone–dextrose at 37 °C to an OD_{600} of ∼0.6. Total RNA from three biological replicates of each strain was isolated using the hot phenol method. snoRNAs were separated on 8% acrylamide/urea gels, transferred to Hybond nylon membranes (GE Healthcare), and probed as indicated. Bands were quantified using Image Lab software (Bio-Rad).

Data Availability. Data from the RiboMethSeq analysis are deposited in the European Nucleotide Archive under accession number PRJEB49663. All other study data are included in the article and/or *SI Appendix*.

Author affiliations: [a]Department of Biochemistry, Emory University School of Medicine, Atlanta, GA 30322; [b]Graduate Program in Biochemistry, Cell and Developmental Biology, Emory University, Atlanta, GA 30322; [c]UMS2008 IBSLor, CNRS-INSERM, Université de Lorraine, Vandoeuvre-les-Nancy 54505, France; and [d]UMR7365 IMoPA, CNRS-Biopôle, Université de Lorraine, Vandoeuvre-les-Nancy 54505, France

1. M. Helm, Post-transcriptional nucleotide modification and alternative folding of RNA. *Nucleic Acids Res.* **34**, 721–733 (2006).
2. I. A. Roundtree, M. E. Evans, T. Pan, C. He, Dynamic RNA modifications in gene expression regulation. *Cell* **169**, 1187–1200 (2017).
3. L. Ayadi, A. Galvanin, F. Pichot, V. Marchand, Y. Motorin, RNA ribose methylation (2′-O-methylation): Occurrence, biosynthesis and biological functions. *Biochim. Biophys. Acta. Gene Regul. Mech.* **1862**, 253–269 (2019).
4. K. E. Sloan *et al.*, Tuning the ribosome: The influence of rRNA modification on eukaryotic ribosome biogenesis and function. *RNA Biol.* **14**, 1138–1152 (2017).
5. P. L. Monaco, V. Marcel, J. J. Diaz, F. Catez, 2′-O-methylation of ribosomal RNA: Towards an epitranscriptomic control of translation? *Biomolecules* **8**, 106 (2018).
6. S. K. Natchiar, A. G. Myasnikov, H. Kratzat, I. Hazemann, B. P. Klaholz, Visualization of chemical modifications in the human 80S ribosome structure. *Nature* **551**, 472–477 (2017).
7. W. A. Decatur, M. J. Fournier, rRNA modifications and ribosome function. *Trends Biochem. Sci.* **27**, 344–351 (2002).
8. D. G. Dimitrova, L. Teysset, C. Carré, RNA 2′-O-methylation (nm) modification in human diseases. *Genes (Basel)* **10**, 117 (2019).
9. S. K. Natchiar, A. G. Myasnikov, I. Hazemann, B. P. Klaholz, Visualizing the role of 2′-OH rRNA methylations in the human ribosome structure. *Biomolecules* **8**, 125 (2018).
10. Y. S. Polikanov, S. V. Melnikov, D. Söll, T. A. Steitz, Structural insights into the role of rRNA modifications in protein synthesis and ribosome assembly. *Nat. Struct. Mol. Biol.* **22**, 342–344 (2015).
11. K. Jack *et al.*, rRNA pseudouridylation defects affect ribosomal ligand binding and translational fidelity from yeast to human cells. *Mol. Cell* **44**, 660–666 (2011).
12. J. Jiang, H. Seo, C. S. Chow, Post-transcriptional modifications modulate rRNA structure and ligand interactions. *Acc. Chem. Res.* **49**, 893–901 (2016).
13. M. McMahon *et al.*, A single H/ACA small nucleolar RNA mediates tumor suppression downstream of oncogenic RAS. *eLife* **8**, e48847 (2019).
14. H. Abou Assi *et al.*, 2′-O-methylation can increase the abundance and lifetime of alternative RNA conformational states. *Nucleic Acids Res.* **48**, 12365–12379 (2020).
15. P. Auffinger, E. Westhof, Rules governing the orientation of the 2′-hydroxyl group in RNA. *J. Mol. Biol.* **274**, 54–63 (1997).
16. G. Kawai *et al.*, Conformational rigidity of specific pyrimidine residues in tRNA arises from posttranscriptional modifications that enhance steric interaction between the base and the 2′-hydroxyl group. *Biochemistry* **31**, 1040–1046 (1992).
17. E. Malek-Adamian *et al.*, Adjusting the structure of 2′-modified nucleosides and oligonucleotides via C4′-α-F or C4′-α-OMe substitution: Synthesis and conformational analysis. *J. Org. Chem.* **83**, 9839–9849 (2018).
18. D. M. Cheng, R. H. Sarma, Nuclear magnetic resonance study of the impact of ribose 2′-O-methylation on the aqueous solution conformation of cytidylyl-(3′ leads to 5′)-cytidine. *Biopolymers* **16**, 1687–1711 (1977).
19. S. K. Mahto, C. S. Chow, Synthesis and solution conformation studies of the modified nucleoside N^4,2′-O-dimethylcytidine (m^{4}Cm) and its analogues. *Bioorg. Med. Chem.* **16**, 8795–8800 (2008).
20. C. S. Chow, T. N. Lamichhane, S. K. Mahto, Expanding the nucleotide repertoire of the ribosome with post-transcriptional modifications. *ACS Chem. Biol.* **2**, 610–619 (2007).
21. Z. Kiss-László, Y. Henry, J. P. Bachellerie, M. Caizergues-Ferrer, T. Kiss, Site-specific ribose methylation of preribosomal RNA: A novel function for small nucleolar RNAs. *Cell* **85**, 1077–1088 (1996).
22. J. P. Bachellerie, J. Cavaillé, Guiding ribose methylation of rRNA. *Trends Biochem. Sci.* **22**, 257–261 (1997).
23. G. Yu, Y. Zhao, H. Li, The multistructural forms of box C/D ribonucleoprotein particles. *RNA* **24**, 1625–1633 (2018).
24. A. Lapinaite *et al.*, The structure of the box C/D enzyme reveals regulation of RNA methylation. *Nature* **502**, 519–523 (2013).
25. J. Lin *et al.*, Structural basis for site-specific ribose methylation by box C/D RNA protein complexes. *Nature* **469**, 559–563 (2011).
26. N. J. Watkins, M. T. Bohnsack, The box C/D and H/ACA snoRNPs: Key players in the modification, processing and the dynamic folding of ribosomal RNA. *Wiley Interdiscip. Rev. RNA* **3**, 397–414 (2012).
27. S. Massenet, E. Bertrand, C. Verheggen, Assembly and trafficking of box C/D and H/ACA snoRNPs. *RNA Biol.* **14**, 680–692 (2017).
28. J. Erales *et al.*, Evidence for rRNA 2′-O-methylation plasticity: Control of intrinsic translational capabilities of human ribosomes. *Proc. Natl. Acad. Sci. U.S.A.* **114**, 12934–12939 (2017).
29. S. Sharma, V. Marchand, Y. Motorin, D. L. J. Lafontaine, Identification of sites of 2′-O-methylation vulnerability in human ribosomal RNAs by systematic mapping. *Sci. Rep.* **7**, 11490 (2017).
30. J. Yang *et al.*, Mapping of complete set of ribose and base modifications of yeast rRNA by RP-HPLC and mung bean nuclease assay. *PLoS One* **11**, e0168873 (2016).
31. U. Birkedal *et al.*, Profiling of ribose methylations in RNA by high-throughput sequencing. *Angew. Chem. Int. Ed. Engl.* **54**, 451–455 (2015).
32. V. Marchand, F. Blanloeil-Oillo, M. Helm, Y. Motorin, Illumina-based RiboMethSeq approach for mapping of 2′-O-Me residues in RNA. *Nucleic Acids Res.* **44**, e135 (2016).
33. M. Taoka *et al.*, Landscape of the complete RNA chemical modifications in the human 80S ribosome. *Nucleic Acids Res.* **46**, 9289–9298 (2018).
34. M. Taoka *et al.*, The complete chemical structure of *Saccharomyces cerevisiae* rRNA: Partial pseudouridylation of U2345 in 25S rRNA by snoRNA snR9. *Nucleic Acids Res.* **44**, 8951–8961 (2016).
35. N. Krogh *et al.*, Profiling of 2′-O-Me in human rRNA reveals a subset of fractionally modified positions and provides evidence for ribosome heterogeneity. *Nucleic Acids Res.* **44**, 7884–7895 (2016).
36. Y. Motorin, M. Quinternet, W. Rhalloussi, V. Marchand, Constitutive and variable 2′-O-methylation (Nm) in human ribosomal RNA. *RNA Biol.* **18**, 88–97 (2021).
37. M. B. Ferretti, K. Karbstein, Does functional specialization of ribosomes really exist? *RNA* **25**, 521–538 (2019).
38. V. Marcel *et al.*, Ribosomal RNA 2′O-methylation as a novel layer of inter-tumour heterogeneity in breast cancer. *NAR Cancer* **2**, zcaa036 (2020).
39. J. Hebras, N. Krogh, V. Marty, H. Nielsen, J. Cavaillé, Developmental changes of rRNA ribose methylations in the mouse. *RNA Biol.* **17**, 150–164 (2020).
40. V. Marcel *et al.*, p53 acts as a safeguard of translational control by regulating fibrillarin and rRNA methylation in cancer. *Cancer Cell* **24**, 318–330 (2013).
41. G. R. R. Aquino *et al.*, RNA helicase-mediated regulation of snoRNP dynamics on pre-ribosomes and rRNA 2′-O-methylation. *Nucleic Acids Res.* **49**, 4066–4084 (2021).
42. Y. Zhao, J. Rai, H. Yu, H. Li, Pseudouridine-free ribosome exhibits distinct inter-subunit movements. bioRxiv [Preprint] (2021). 10.1101/2021.06.02.446812 (Accessed 19 December 2021).
43. D. Tollervey, H. Lehtonen, M. Carmo-Fonseca, E. C. Hurt, The small nucleolar RNP protein NOP1 (fibrillarin) is required for pre-rRNA processing in yeast. *EMBO J.* **10**, 573–583 (1991).
44. D. Tollervey, H. Lehtonen, R. Jansen, H. Kern, E. C. Hurt, Temperature-sensitive mutations demonstrate roles for yeast fibrillarin in pre-rRNA processing, pre-rRNA methylation, and ribosome assembly. *Cell* **72**, 443–457 (1993).
45. M. A. Amin *et al.*, Fibrillarin, a nucleolar protein, is required for normal nuclear morphology and cellular growth in HeLa cells. *Biochem. Biophys. Res. Commun.* **360**, 320–326 (2007).
46. F. J. LaRiviere, S. E. Cole, D. J. Ferullo, M. J. Moore, A late-acting quality control process for mature eukaryotic rRNAs. *Mol. Cell* **24**, 619–626 (2006).
47. P. Tessarz *et al.*, Glutamine methylation in histone H2A is an RNA-polymerase-I-dedicated modification. *Nature* **505**, 564–568 (2014).
48. W. T. Peng *et al.*, A panoramic view of yeast noncoding RNA processing. *Cell* **113**, 919–933 (2003).
49. A. Paul *et al.*, Bcd1p controls RNA loading of the core protein Nop58 during C/D box snoRNP biogenesis. *RNA* **25**, 496–506 (2019).
50. S. Khoshnevis, R. E. Dreggors, T. F. R. Hoffmann, H. Ghalei, A conserved Bcd1 interaction essential for box C/D snoRNP biogenesis. *J. Biol. Chem.* **294**, 18360–18371 (2019).
51. A. Baudin-Baillieu *et al.*, Nucleotide modifications in three functionally important regions of the *Saccharomyces cerevisiae* ribosome affect translation accuracy. *Nucleic Acids Res.* **37**, 7665–7677 (2009).
52. X. H. Liang, Q. Liu, M. J. Fournier, rRNA modifications in an intersubunit bridge of the ribosome strongly affect both ribosome biogenesis and activity. *Mol. Cell* **28**, 965–977 (2007).
53. E. W. Mills, R. Green, Ribosomopathies: There's strength in numbers. *Science* **358**, eaan2755 (2017).
54. S. O. Sulima, I. J. F. Hofman, K. De Keersmaecker, J. D. Dinman, How ribosomes translate cancer. *Cancer Discov.* **7**, 1069–1087 (2017).
55. Y. Yi *et al.*, A PRC2-independent function for EZH2 in regulating rRNA 2′-O methylation and IRES-dependent translation. *Nat. Cell Biol.* **23**, 341–354 (2021).
56. J. W. Harger, J. D. Dinman, An in vivo dual-luciferase assay system for studying translational recoding in the yeast *Saccharomyces cerevisiae*. *RNA* **9**, 1019–1024 (2003).
57. Y. N. Cheung *et al.*, Dissociation of eIF1 from the 40S ribosomal subunit is a key step in start codon selection in vivo. *Genes Dev.* **21**, 1217–1230 (2007).
58. K. M. Keeling *et al.*, Leaky termination at premature stop codons antagonizes nonsense-mediated mRNA decay in S. cerevisiae. *RNA* **10**, 691–703 (2004).
59. J. Salas-Marco, D. M. Bedwell, Discrimination between defects in elongation fidelity and termination efficiency provides mechanistic insights into translational readthrough. *J. Mol. Biol.* **348**, 801–815 (2005).
60. D. M. Landry, M. I. Hertz, S. R. Thompson, RPS25 is essential for translation initiation by the Dicistroviridae and hepatitis C viral IRESs. *Genes Dev.* **23**, 2753–2764 (2009).
61. N. Garreau de Loubresse *et al.*, Structural basis for the inhibition of the eukaryotic ribosome. *Nature* **513**, 517–522 (2014).
62. P. Qin, D. Yu, X. Zuo, P. V. Cornish, Structured mRNA induces the ribosome into a hyper-rotated state. *EMBO Rep.* **15**, 185–190 (2014).
63. J. Choi, S. O'Loughlin, J. F. Atkins, J. D. Puglisi, The energy landscape of -1 ribosomal frameshifting. *Sci. Adv.* **6**, eaax6969 (2020).
64. J. Chen *et al.*, Dynamic pathways of -1 translational frameshifting. *Nature* **512**, 328–332 (2014).
65. P. R. Bhatt *et al.*, Structural basis of ribosomal frameshifting during translation of the SARS-CoV-2 RNA genome. *Science* **372**, 1306–1313 (2021).
66. S. O. Sulima *et al.*, Eukaryotic rpL10 drives ribosomal rotation. *Nucleic Acids Res.* **42**, 2049–2063 (2014).
67. A. Meskauskas, J. D. Dinman, Ribosomal protein L3: Gatekeeper to the A site. *Mol. Cell* **25**, 877–888 (2007).
68. R. Belardinelli, H. Sharma, F. Peske, W. Wintermeyer, M. V. Rodnina, Translocation as continuous movement through the ribosome. *RNA Biol.* **13**, 1197–1203 (2016).
69. M. C. Justice *et al.*, Elongation factor 2 as a novel target for selective inhibition of fungal protein synthesis. *J. Biol. Chem.* **273**, 3148–3151 (1998).
70. H. Huang, K. Karbstein, Assembly factors chaperone ribosomal RNA folding by isolating helical junctions that are prone to misfolding. *Proc. Natl. Acad. Sci. U.S.A.* **118**, e2101164118 (2021).
71. M. Kofoed *et al.*, An updated collection of sequence barcoded temperature-sensitive alleles of yeast essential genes. *G3 (Bethesda)* **5**, 1879–1887 (2015).
72. D. Maag, C. A. Fekete, Z. Gryczynski, J. R. Lorsch, A conformational change in the eukaryotic translation preinitiation complex and release of eIF1 signal recognition of the start codon. *Mol. Cell* **17**, 265–275 (2005).
73. L. A. Passmore *et al.*, The eukaryotic translation initiation factors eIF1 and eIF1A induce an open conformation of the 40S ribosome. *Mol. Cell* **26**, 41–50 (2007).
74. T. V. Pestova, V. G. Kolupaeva, The roles of individual eukaryotic translation initiation factors in ribosomal scanning and initiation codon selection. *Genes Dev.* **16**, 2906–2922 (2002).
75. J. S. Nanda *et al.*, eIF1 controls multiple steps in start codon recognition during eukaryotic translation initiation. *J. Mol. Biol.* **394**, 268–285 (2009).
76. D. Maag, J. R. Lorsch, Communication between eukaryotic translation initiation factors 1 and 1A on the yeast small ribosomal subunit. *J. Mol. Biol.* **330**, 917–924 (2003).
77. J. Dong *et al.*, Rps3/uS3 promotes mRNA binding at the 40S ribosome entry channel and stabilizes preinitiation complexes at start codons. *Proc. Natl. Acad. Sci. U.S.A.* **114**, E2126–E2135 (2017).

78. A. G. Hinnebusch, The scanning mechanism of eukaryotic translation initiation. *Annu. Rev. Biochem.* **83**, 779–812 (2014).
79. A. G. Hinnebusch, Structural insights into the mechanism of scanning and start codon recognition in eukaryotic translation initiation. *Trends Biochem. Sci.* **42**, 589–611 (2017).
80. J. L. Llácer *et al.*, Conformational differences between open and closed states of the eukaryotic translation initiation complex. *Mol. Cell* **59**, 399–412 (2015).
81. D. Nachmani *et al.*, Germline NPM1 mutations lead to altered rRNA 2′-O-methylation and cause dyskeratosis congenita. *Nat. Genet.* **51**, 1518–1529 (2019).
82. F. Zhou *et al.*, AML1-ETO requires enhanced C/D box snoRNA/RNP formation to induce self-renewal and leukaemia. *Nat. Cell Biol.* **19**, 844–855 (2017).
83. S. Ojha, S. Malla, S. M. Lyons, snoRNPs: Functions in ribosome biogenesis. *Biomolecules* **10**, 783 (2020).
84. S. Parker *et al.*, Large-scale profiling of noncoding RNA function in yeast. *PLoS Genet.* **14**, e1007253 (2018).
85. L. N. Balarezo-Cisneros *et al.*, Functional and transcriptional profiling of non-coding RNAs in yeast reveal context-dependent phenotypes and in trans effects on the protein regulatory network. *PLoS Genet.* **17**, e1008761 (2021).
86. J. Esguerra, J. Warringer, A. Blomberg, Functional importance of individual rRNA 2′-O-ribose methylations revealed by high-resolution phenotyping. *RNA* **14**, 649–656 (2008).
87. X. H. Liang, Q. Liu, M. J. Fournier, Loss of rRNA modifications in the decoding center of the ribosome impairs translation and strongly delays pre-rRNA processing. *RNA* **15**, 1716–1728 (2009).
88. S. D. Kulkarni *et al.*, Temperature-dependent regulation of upstream open reading frame translation in S. cerevisiae. *BMC Biol.* **17**, 101 (2019).
89. F. Zhou, H. Zhang, S. D. Kulkarni, J. R. Lorsch, A. G. Hinnebusch, eIF1 discriminates against suboptimal initiation sites to prevent excessive uORF translation genome-wide. *RNA* **26**, 419–438 (2020).
90. G. Monteuuis *et al.*, Non-canonical translation initiation in yeast generates a cryptic pool of mitochondrial proteins. *Nucleic Acids Res.* **47**, 5777–5791 (2019).
91. T. von der Haar, J. E. McCarthy, Intracellular translation initiation factor levels in *Saccharomyces cerevisiae* and their role in cap-complex function. *Mol. Microbiol.* **46**, 531–544 (2002).
92. D. Maag, M. A. Algire, J. R. Lorsch, Communication between eukaryotic translation initiation factors 5 and 1A within the ribosomal pre-initiation complex plays a role in start site selection. *J. Mol. Biol.* **356**, 724–737 (2006).
93. F. Pichot *et al.*, Holistic optimization of bioinformatic analysis pipeline for detection and quantification of 2′-O-methylations in RNA by RiboMethSeq. *Front. Genet.* **11**, 38 (2020).
94. L. Valásek, B. Szamecz, A. G. Hinnebusch, K. H. Nielsen, In vivo stabilization of preinitiation complexes by formaldehyde cross-linking. *Methods Enzymol.* **429**, 163–183 (2007).
95. M. G. Acker, S. E. Kolitz, S. F. Mitchell, J. S. Nanda, J. R. Lorsch, Reconstitution of yeast translation initiation. *Methods Enzymol.* **430**, 111–145 (2007).